

FRONTIER LETTER

Open Access



# Tectonic significance of the 2021 Lamjung, Nepal, mid-crustal seismic cluster

Bharat Prasad Koirala<sup>1\*</sup>, Marine Laporte<sup>2</sup> , Laurent Bollinger<sup>2\*</sup> , Daria Batteux<sup>1,2</sup>, Jean Letort<sup>3</sup> , Aurélie Guilhem Trilla<sup>2</sup> , Nicolas Wendling-Vazquez<sup>2</sup>, Mukunda Bhattarai<sup>1</sup>, Shiba Subedi<sup>4</sup>  and Lok Bijaya Adhikari<sup>1</sup> 

## Abstract

Since the  $M_w$  7.9 Gorkha earthquake of April 25, 2015, the seismicity of central and western Nepalese Himalaya has been monitored by an increasing number of permanent seismic stations. These instruments contribute to the location of thousands of aftershocks that occur at the western margin of the segment of the Main Himalayan Thrust (MHT) that ruptured in 2015. They also help to constrain the location of seismic clusters that originated at the periphery of the fault ruptured by the Gorkha earthquake, which may indicate a migration of seismicity along the fault system. We report here a seismic crisis that followed the Lamjung earthquake, a moderate  $M_w$  4.7 event ( $M_L$  5.8,  $M_{LV}$  5.3) that occurred on May 18, 2021, about 30 km west of the Gorkha earthquake epicenter at the down-dip end of the locked fault zone. The study of the hypocentral location of the mainshock and its first 117 aftershocks confirms mid-crustal depths and supports the activation of a 30–40° dipping fault plane, possibly associated with the rupture of the updip end of the MHT mid-crustal ramp. The cluster of aftershocks occurs near the upper decollement of the thrust system, probably in its hanging wall, and falls on the immediate northern margin of a region of the fault that has not been ruptured since the 1344 or 1505 CE earthquake. The spatio-temporal distribution of the first 117 aftershocks shows a typical decrease in the associated seismicity rate and possible migration of seismic activity. Since then, the local seismicity has returned to the pre-earthquake rate and careful monitoring has not revealed any large-scale migration of seismicity towards the locked fault segments.

**Keywords** Earthquake, Clustered seismicity, Main Himalayan Thrust, Himalaya, Nepal

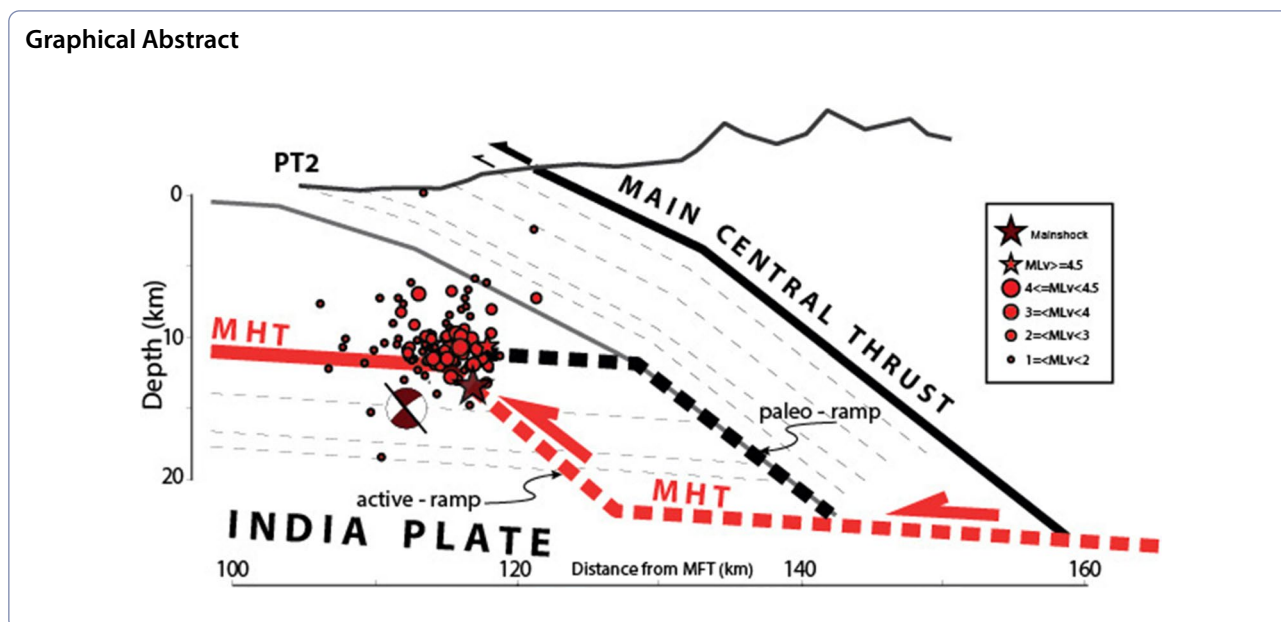
\*Correspondence:

Bharat Prasad Koirala  
koirala\_bharat@yahoo.com  
Laurent Bollinger  
Laurent.bollinger@cea.fr

Full list of author information is available at the end of the article



© The Author(s) 2023. **Open Access** This article is licensed under a Creative Commons Attribution 4.0 International License, which permits use, sharing, adaptation, distribution and reproduction in any medium or format, as long as you give appropriate credit to the original author(s) and the source, provide a link to the Creative Commons licence, and indicate if changes were made. The images or other third party material in this article are included in the article's Creative Commons licence, unless indicated otherwise in a credit line to the material. If material is not included in the article's Creative Commons licence and your intended use is not permitted by statutory regulation or exceeds the permitted use, you will need to obtain permission directly from the copyright holder. To view a copy of this licence, visit <http://creativecommons.org/licenses/by/4.0/>.



## Introduction

Nepal is exposed to large ( $M7+$ ) and great ( $M8+$ ) devastating earthquakes that partially or completely rupture the updip locked segments of the Main Himalayan Thrust (MHT) identified as the plate boundary fault that accommodates the shortening between India and the Tibetan Plateau (e.g., Avouac 2003; Bilham 2019; Dal Zilio et al. 2021). The most recent of these very strong earthquakes is the April 25, 2015  $M_w$  7.9 Gorkha earthquake, which ruptured a  $140 \times 50$  km locked fault segment in central Nepal (e.g., Avouac et al. 2015; Grandin et al. 2015), and was followed by tens of thousands of aftershocks (e.g., Adhikari et al. 2015; 2023; Bai et al. 2019; Letort et al. 2016; Mendoza et al. 2019; Yamada et al. 2020). In addition to these rare strong earthquakes, moderate seismic sources (local magnitude  $M_L$  4+) occur frequently, exposing areas close to the epicenter to strong ground motion and possible damage.

The Department of Mines and Geology (DMG) in Nepal is the only government organization responsible for rapidly locating and disseminating information about these earthquakes to government authorities and the public. Since 1994, it has been providing earthquake-related information (location and magnitude) to the Ministry Of Home Affairs (MOHA), Ministry Of Industry Commerce and Supplies (MOICS) and since its inception to the National Disaster Risk Reduction and Management Authority (NDRRMA) after every  $M_L$  4+ event. Indeed, most of these earthquakes occur at mid-crustal or shallower depths, near and above the MHT decollement (Pandey et al. 1995; Hoste-Colomer et al. 2018; Laporte et al. 2021), and are likely to be felt by the population.

Between 1994 and 25 April 2015, the date of the large  $M_w$  7.9 Gorkha earthquake, 390 of these alerts were delivered to the authorities. Since the Gorkha earthquake, tens of thousands of lower magnitude earthquakes have been detected and located under the national seismological network (Adhikari et al. 2015, 2023; Baillard et al. 2017). Of these earthquakes, most with magnitudes below  $M_L$  4, 645 new alerts were provided to the authorities and to the public.

This article focuses on one of these recent earthquakes that triggered the seismic alert. This event in particular is chosen because of its location, its position within a larger spatio-temporal sequence of seismic events, and more generally because of its seismotectonic interest.

On May 18, 2021 at 23:57 UTC (5:42 local time), a moderate  $M_L$  5.8 earthquake shook central-western Nepal from Pokhara to Kathmandu (Fig. 1), within 100 km of the macroseismic epicenter, and was felt up to 400 km away in Rae Bareli and Lucknow in India (EMSC felt reports <https://www.emsc-csem.org>). The mainshock damaged more than 200 houses and injured 6 people. It was followed by an  $M_L$  5.3 earthquake less than 3 h later and by 4 more aftershocks of magnitude greater than 4 within the next 24 h (Table 1). All of these earthquakes were widely felt by the local population. Several smaller earthquakes were also felt around the villages of Lamjung–Besisahar in the Marsyangdi valley, demonstrating the relatively shallow depth of the seismic sources.

In this paper we study the Lamjung mainshock and subsequent seismic sequence using the Nepalese Seismological Network. We relocate the events of the seismic sequence using various techniques, and discuss their

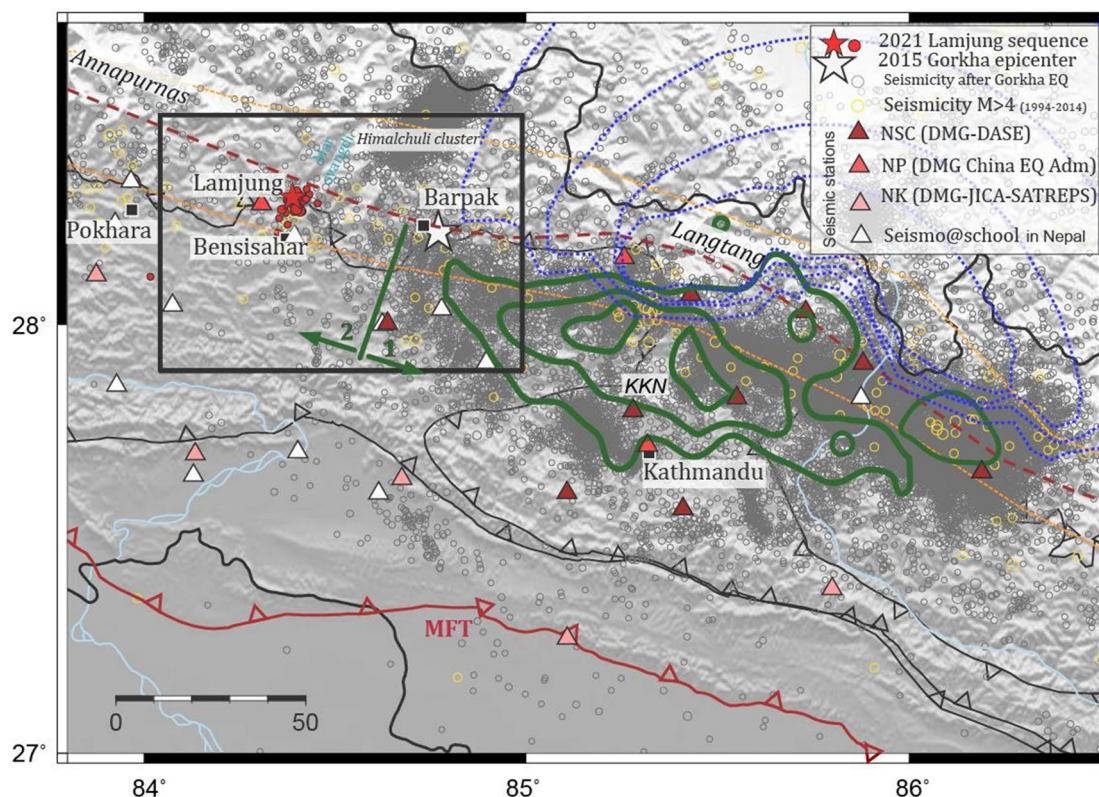


**Fig. 1** Seismicity map of the 2021 Lamjung seismic sequence (red circles) in central Nepal. The triangles materialize the seismic stations used in this study. Grey circles: epicenters of the earthquakes that happened after the Gorkha earthquake (NEMRC catalogue 2020). Yellow circles: earthquakes that triggered the seismic alarm before Gorkha earthquake. Thick dark green polylines correspond to the 2 m isocontours of the Gorkha earthquake slip at depth (Grandin et al. 2015). The dark green segment with double arrows roughly separates the segment of Main Himalayan Thrust ruptured (1) and unruptured (2) during the 2015 Gorkha earthquake, and was drawn after confronting the source models of Gorkha earthquake and the catalogue of aftershocks (Adhikari et al. 2023). Blue dashed polylines correspond to the 10 cm isocontours of the afterslip (Zhao et al. 2017). *KKN* Kakani seismological station

implications. Finally, we place them in their regional structural scheme to provide some seismotectonic interpretations.

**Table 1** Parameters of the largest earthquakes that triggered the seismic alarm at NEMRC

Date	Time	Latitude	Longitude	Magnitude $M_L$
B.S:2078-2-5	Local: 05:42	28.28	84.39	5.8
A.D:2021-05-18	UTC: 23:57			
B.S:2078-2-5	Local: 08:16	28.26	84.35	4.0
A.D:2021-05-19	UTC: 02:31			
B.S:2078-2-5	Local: 08:17	28.26	84.36	4.1
A.D:2021-05-19	UTC: 02:32			
B.S:2078-2-5	Local: 08:26	28.27	84.40	5.3
A.D:2021-05-19	UTC: 02:41			
B.S:2078-2-5	Local: 21:23	28.27	84.42	4.0
A.D:2021-05-19	UTC: 15:38			
B.S:2078-2-5	Local: 22:39	28.24	84.41	4.5
A.D:2021-05-19	UTC: 16:54			

**Seismotectonic setting of central western Nepal**

As elsewhere along the Himalayas, the tectonic wedge of central-western Nepal is the result of the continental subduction of the India Plate beneath the Tibetan Plateau. The main active thrust fault that underlies the wedge and accommodates the regional shortening is the Main Himalayan Thrust (MHT). This major intercontinental thrust system was first described by geologists a century ago (e.g., Argand 1922) and has been fully documented in central western Nepal since then. The at-depth geometry of the MHT has been materialized recently by several geophysical techniques, including gravimetry (e.g., Cattin et al. 2001), and active and passive seismic imaging (Hauck et al. 1998; Nabelek et al. 2009). The subduction of the India plate beneath Nepal is highlighted by

the shallow north-dipping Moho (e.g., Schulte-Pelkum et al. 2005; Nabelek et al. 2009; He et al. 2018). The fault itself was first imaged elsewhere in the eastern Himalayas by seismic reflection during the Indepth project (Hauck et al. 1998). In central Nepal, close to the area of interest in this paper, a mid-crustal low-velocity zone (LVZ) has been mapped by passive seismic imaging (Nabelek et al. 2009; Duputel et al. 2016). This LVZ extends for several tens of kilometers, at distances between 50 and 90 km from the front, and is interpreted by the authors to be associated with the presence of the MHT shear zone, possibly injected by fluids. This LVZ is the upper “flat” of a structure often described by geologists as a flat–ramp–flat, with a ramp inferred by antiformal stacking of tectonic units scrapped off the India Plate.

Several faults, that are surface expressions of the Himalayan thrust system, merge at depth on the MHT, including, from south to north, the Main Frontal, Main Boundary and Main Central Thrusts (MFT, MBT and MCT, respectively, e.g., Upreti et al. 1999). The MFT separates the sediments of the Molassic basins of northern India from a fold and thrust belt at the front of the range, the Siwaliks foothills, formed mainly of Pliocene siltstones, sandstones and conglomerates. Further north, the MBT separates the Siwaliks from the Lesser Himalayas, which consist of a stack of tectonic slivers of meta-sedimentary rocks of India Plate origin. Documentation of several balanced cross sections in central and western Nepal shows significant lateral variations of large anti-formal stacks that developed in the hanging wall of the MHT, near the main ramp of the thrust system (e.g., Robinson and Martin 2014; Ghoshal et al. 2023). Finally, further north, the MCT Zone separates this lesser Himalaya from crystalline formations that are well exposed at the front of the high mountain range.

The present shortening of the Himalayas, accommodated deep below the high topography, is transmitted at the MFT, at Holocene displacement rates similar to the slip rates, leaving only marginal slip potential for out-of-sequence thrusting and internal shortening (Lavé and Avouac 2001). The GNSS velocity field shows that the MHT alone accommodates almost half of the 4 cm/year shortening between India and stable Eurasia. The remainder is accommodated by block extrusion and local thrusting further north. More than estimating total shortening, continuous GNSS data in central western Nepal, locally supplemented by levelling and InSAR, help constrain the interseismic coupling of the MHT. The MHT appears to be locked in central western Nepal, as it is throughout the Himalayas, over a width of more than 80 km. As elsewhere, the locking is complete and is responsible for the strong earthquakes that nucleate near the down-dip

end of the locked zone, near the brittle–ductile transition (Ader et al. 2012; Grandin et al. 2012; Ingleby et al. 2020).

Intense mid-crustal seismicity develops in this region at mid-crustal depths (Pandey et al. 1995); this seismicity is interpreted as resulting from stress build-up (e.g., Cattin and Avouac 2000; Bollinger et al. 2004; Ader et al. 2012). The study of this seismicity in the trace of the Gorkha earthquake reveals lateral heterogeneities, that are perennial on the scale of the seismic cycle and are thought to reflect the lateral variations of mid-crustal structures, en-echelon ramps, and tear faults between ramp segments (e.g., Hoste-colomer et al. 2017), which act as many geometric heterogeneities of the main ramp system, receiver faults of the stress that builds up at depth during the interseismic period. Studying the seismic swarms within this region, along the down-dip end of the locked fault zone, is therefore critical to improving our understanding of the seismic behavior along the thrust system (Hoste-Colomer et al. 2018), and its seismogenic potential (e.g., Michel et al. 2021).

## Data and methods

### Seismic monitoring

The seismic bulletin of the Lamjung earthquake sequence is produced by manually picking P- and S-wave onsets in seismic signals from a total of 41 seismic stations available in central and western Nepal. Of these, 11 stations were deployed under the DMG-Département Analyse Surveillance Environnement—France (DASE) collaboration: 8 1-Hz vertical short-period seismometers and 3 CMG-3T Güralp broadband 3-component seismometers, including the KKN station which is shared in real time and distributed by IRIS. In addition, 8 stations from the Nepal–Japan collaboration supported by the SATREPS program of JICA/JST and 5 stations from the DMG-China Earthquake Administration collaboration contributed in real time during the earthquake crisis. 16 vertical component RaspberryShake instruments from the Nepal School Seismology Network (Subedi et al. 2020a; 2020b) complement these stations.

### Operational earthquake detection and preliminary location

Two geophysical workflows are used in parallel at National Earthquake Monitoring and Research Center—Nepal (NEMRC) to study seismic clusters: (1) Jade-Onyx, which uses only the 11 historical stations from the DMG-DASE collaboration, but benefits from 20 years of experience of NEMRC seismic analysts and a large historical database of waveforms and (2) Seiscomp3 (Weber et al. 2007), which takes advantage of all available Nepalese seismological stations mentioned above. This workflow is

implemented with several alternative earthquake locators (see Sect. “Earthquake relocation” for details).

A common velocity model is considered in both workflows. It is the 1D model determined by Pandey (1985), which consists of 3 horizontal layers. The P- and S-wave velocities are 5.56, 6.50, 8.10 and 3.18, 3.71, 4.63 km/s, respectively, with depth boundaries at 0, 23 and 55 km (Pandey 1985; Pandey et al. 1995).

First, we used the local earthquake detector, phase picker, and locator (i.e., LocGSE see e.g., (Duverger et al. 2021)) available under Jade-Onyx to generate a preliminary bulletin with the 11 stations available in this workflow, because of the efficiency of this procedure after years of use by the seismic analysts.

The early locations of the Lamjung 2021 mainshock and the largest aftershocks that triggered the seismic alarm at the Nepalese national center were immediately published on the National Earthquake Monitoring and Research Center (NEMRC) website (<http://seismonepal.gov.np/home>; Table 1).

All the events were located at mid-crustal depths within 5 km of the mainshock hypocenter. Preliminary locations indicated that the cluster occurred in a structural position comparable to the hypocenter of the Gorkha earthquake, but at about 30 km to the west (Adhikari et al. 2015) and at approximately 20 km to the southwest of a large transient cluster, the Himalchuli

cluster, that developed between 2017 and 2019 (Adhikari et al. 2021; 2023) (Figs. 1 and 2). In addition, the mainshock occurred the same week as a cluster of small earthquakes which developed along the western edge of the Gorkha earthquake rupture (Figs. 1 and 2), and in the vicinity of the down-dip end of the locked fault zone of the MHT, locus of its elusive mid-crustal ramp where stress builds up between large earthquakes (e.g., Cattin and Avouac 2000; Bollinger et al. 2004; Lindsey et al. 2018). We have therefore paid particular attention to this Lamjung seismic cluster.

In order to better resolve the earthquake location and learn from the crisis, we complemented the early detections and phase-picks by an automatic picking procedure developed on the signals recorded at all available stations under Seiscomp3. Finally, we manually refined the P and S phase onsets to reduce the time arrival bias introduced by the automatic procedures.

A total of 2317 P- and 1312 S-wave arrivals have been manually picked and contribute to the location of 129 earthquakes that occurred within 14 days of the mainshock (Figs. 2 and 3A).

**Magnitudes and completeness of the seismic catalogue**

In addition to the local magnitude  $M_L$  determined at NEMRC (see e.g., Adhikari et al. 2015), a local magnitude  $M_{L_v}$  is determined for each event at each station

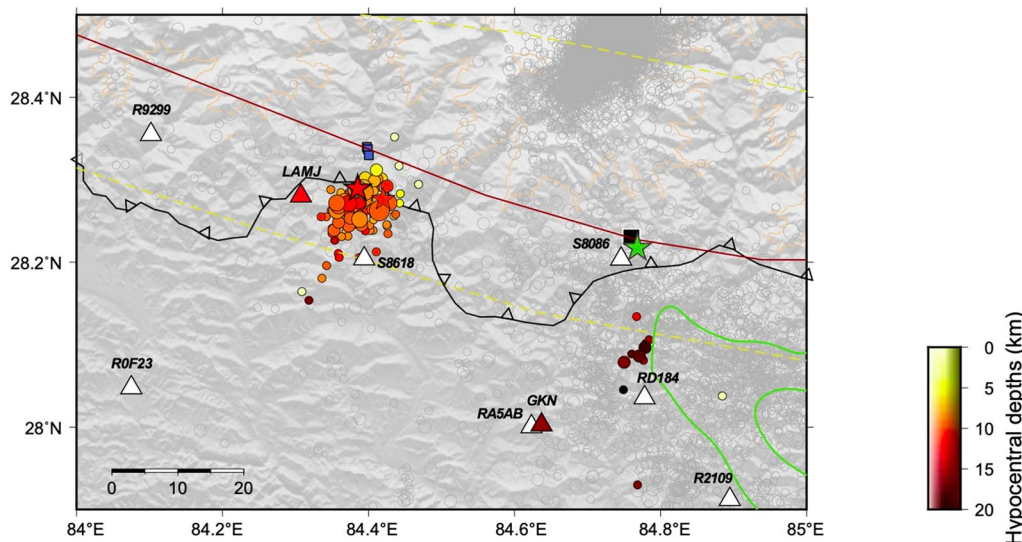


**Fig. 2** Seismicity map of the 2021 Lamjung seismic sequence (colored circles, with colors as a function of hypocentral depth) in central western Nepal. The red line corresponds to the trace of the base of the ramp according to Hubbard et al. 2016, the yellow dashed lines correspond to the modeled down-dip limits at 95% of the coupling across Nepal (Lindsey et al. 2018), The orange line corresponds to the 3500 m iso-altitude, which controls the expression of seismicity along-strike Nepal Himalayas (Bollinger et al. 2004). The blue squares correspond to the location of the Bahundanda hot springs. The green star materializes the epicenter of the Gorkha earthquake, while the green lines locates the 2-m isocontours of the Gorkha earthquake slip at depth (Grandin et al. 2015). The circles in grey locate the epicenter of the earthquakes that happened between April 2015 and May 2021. The triangles correspond to the seismic stations used in this study

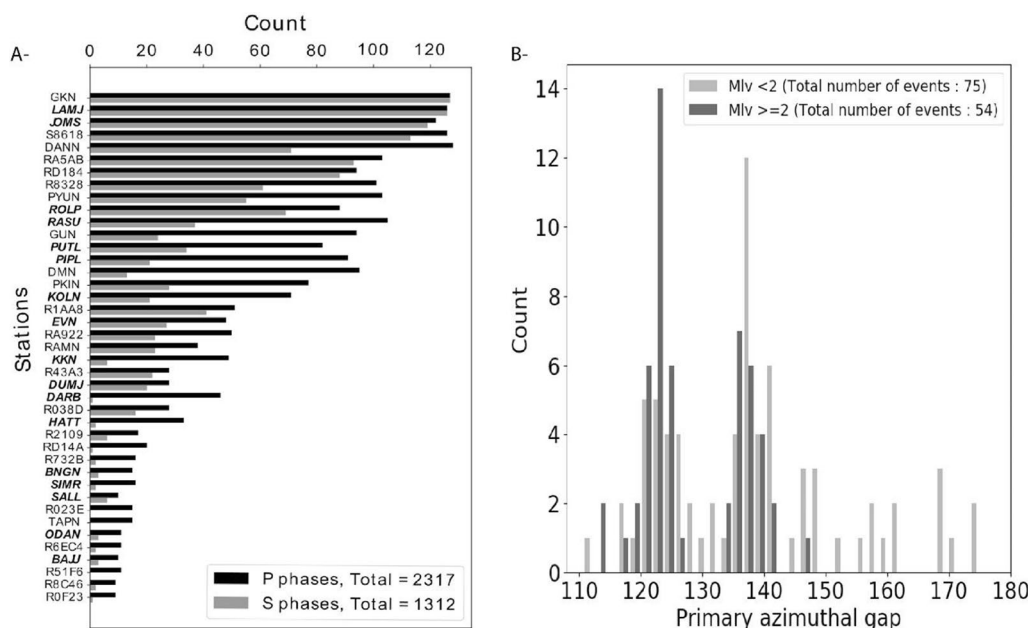


**Fig. 3** A Distribution of the number of P and S phase picks at the stations contributing to the location (3-component stations in bold). B Distribution of the azimuthal gap for the mainshock and its 120 aftershocks

using the Seiscomp3 workflow (Weber et al. 2007), which calculates the classical formula of Richter (1935) at each station:  $M_{Lvi} = \text{Log}(A_i) - \text{Log}(A_0)$ , where  $A_i$  is the maximum zero-to-peak trace amplitude in millimeters measured on the vertical component of stations  $i$  that is filtered in order to replicate the response of a standard Wood–Anderson seismograph. The second term  $\text{Log}(A_0)$  corresponds to the Seiscomp3 default calibration values which are functions of the epicentral distances. The final network magnitude  $M_{Lv}$  is the mean of the magnitudes  $M_{Lvi}$  calculated at all available stations after removing the outliers above the 12.5% percentile.

The Gutenberg–Richter distribution and magnitude histogram (Fig. 4) show a completeness magnitude  $M_c$  of about 1.7, inferred from the decrease in detections below this specific value. Given this completeness magnitude, we estimate the b-value of the magnitude distribution to be  $0.64 \pm 0.07$ , which is a low value for Nepal (Adhikari et al. 2023) as well as for elsewhere.

This anomalously low  $b$ -value during the aftershock series could be representative of the signature of a region of high stress concentration associated with interseismic strain accumulation and redistribution in the vicinity of a locked fault zone, as noted by Nakaya, (2006) (see also Scholz 2015).

### Earthquake relocation and mainshock mechanism

#### Earthquake relocation

The preliminary locations were obtained using Locsat, the locator used for operational purposes in the Seiscomp3 workflow at NEMRC.

We complementarily implement 2 alternative absolute locators, Hypo71 and Nonlinloc, and a double difference relative location procedure with HypoDD.

We selected Hypo71 (Lee and Lahr 1972) because it is a simple, tried-and-tested locator that allows us to reduce the location uncertainties associated with the velocity model by incorporating a weighting scheme for picks as a function of source–station distances, and for the sake of homogeneity with previous works (Adhikari et al. 2023). A full weight is assigned to picks observed at stations within 100 km of the source, and a zero weight is assigned to picks at stations more than 200 km away. Between the two distances, picks are weighted linearly between 0 and 1. We give more weight to the P-phases than to the S-phases and take into account the station elevation by applying an additional time delay as a function of elevation.

Considering the uncertainty in the earthquake location resulting from both network geometry and velocity model uncertainties, we apply a quality criterion to our final seismic locations. Following previous empirical

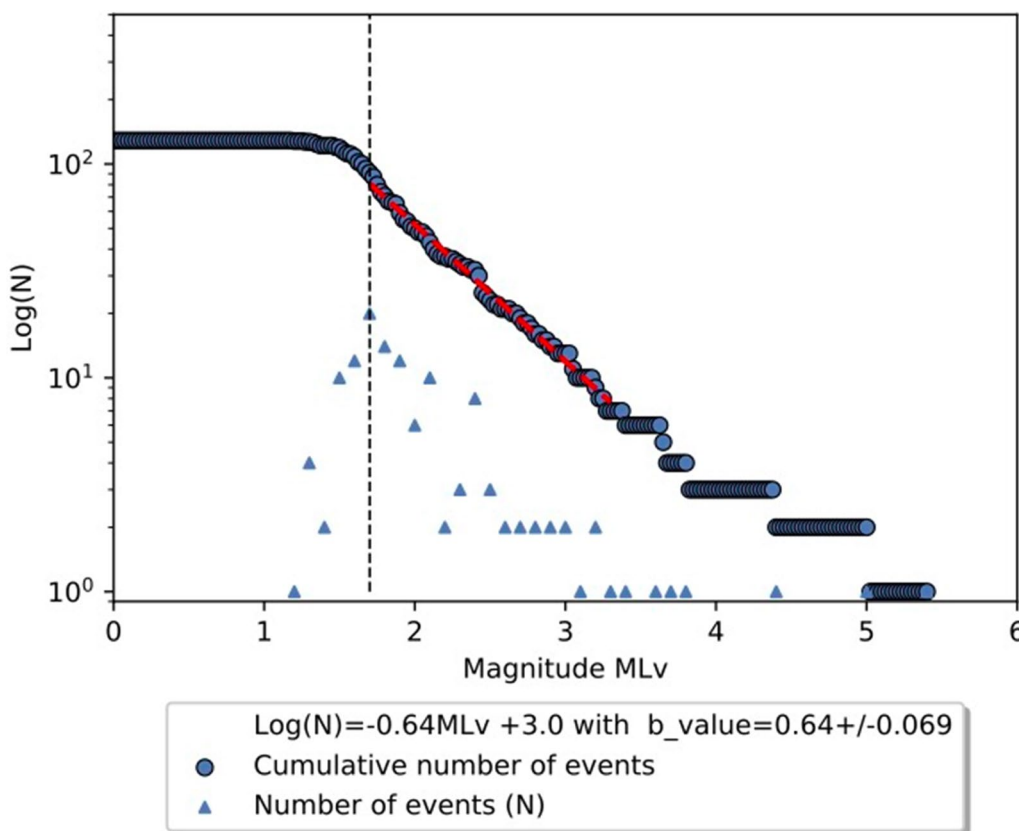


**Fig. 4** Frequency–magnitude distribution of the catalogue of earthquakes of the Lamjung cluster. Completeness magnitude is estimated at  $M_{L_v}$  1.7.

works (e.g., Hoste-Colomer et al. 2018; Laporte et al. 2021), we consider the higher quality locations to be those with a final RMS of less than 0.7 s, horizontal and vertical errors computed by the Hypo71 locator of less than 2 km, and obtained with a minimum of 6 P-phases and 3 S-phases. In total, 44 events meet these criteria.

We then compare these results with locations obtained using NonLinLoc (Lomax et al. 2000; 2009) in order to assess the sensitivity of the results to the locator algorithm. Indeed, the NonLinLoc approach is significantly different in that it avoids the linearization problem by using a grid search algorithm that is able to correctly account for the large differences in station elevations. We computed P-phase travel time tables at each node of an initial grid consisting of 401 nodes spaced every 1 km horizontally and 106 nodes spaced every 1 km vertically around the initial location of the mainshock. S-phase travel times were then derived using a constant  $V_p/V_s$  ratio of 1.75, consistent with the Pandey (1985) velocity model. Recursively, the algorithm returns a preferred hypocentral location where the location residuals are minimized with respect to the posterior probability density function (PDF) at each

node of the 3D grid. The location algorithm follows the inversion approach of Tarantola and Valette (1982) and the PDF is constructed by considering the Equal Differential Time (EDT likelihood function) formulation of Font et al. (2004). An Oct-tree sampling algorithm is preferred to refine the grid recursively by densifying the grid in areas of higher PDF (Lomax et al. 2009). These earthquake location methods provide an absolute location for all 129 events that occurred in the 14 days following the mainshock. Of these 129 events, 117 events are clustered within the Lamjung seismic cluster.

For a better spatial characterization of the cluster, we also used the HypoDD algorithm (Waldhauser and Ellsworth 2000) to obtain relative relocations from the Hypo71 locator of the Seiscomp3 workflow. We processed 1460 phases resulting from a selection of 2256 pairs of P-phases and 1262 pairs of S-phases linked within 255 event pairs with an average of 18 links per pair for a maximum source–station distance of 200 km. We apply an iteration procedure that follows a three-stage iterative scheme consisting of 5 iterations considering only P-phases, 5 iterations considering P-phases and S-phases with half-weight, and finally 10 iterations considering P- and S- phases, a distance cutoff of 5 km

between event pairs and a misfit weighting factor of 4 between event pairs.

### Focal mechanism of the mainshock

To gain insights into the mechanism at the origin of this seismic cluster, we performed regional waveform inversions to determine the moment tensor solution of the mainshock. The continuous data recorded by 8 regional broadband seismic stations distributed between about 80 and 1600 km around the source are used to retrieve the focal mechanism and the associated deviatoric moment tensor of the mainshock following the methodology of the Time-Domain Deviatoric Moment Tensor Inversion (TDMT-INVC) of Dreger 2003. The distribution of the 8 stations around the source provides a fair azimuthal coverage of the source radiation. For each station, the waveforms are deconvolved with the instrumental responses (for Guralp CMG-3T, Streckeisen STS-1H/1 V-VBB, Streckeisen STS-2), integrated to displacement, decimated to 1 point per second, and then filtered between 25 and 50-s period for the Nepalese stations, and between 40 and 80-s period for the other and more distant stations (i.e., LSA and TARG). Considering the distance range, the depth and the frequency bands, the point-source approximation used in the inversion is sufficient to explain the source of the  $M_L$  4.7 Lamjung earthquake. The temporal moment tensor inversion takes into account the three components of the recorded signal per station, and compares the real data with synthetic signals. The synthetic signals are calculated in displacement using the Computer Programs in Seismology (CPS; Herrmann (2013)), and three different velocity models have been tested: CRUST1 (Laske et al. 2013), CRUST2 (Bassin et al. 2000), and CUB (Ritzwoller et al. 2002). These global velocity models were preferred to the local Nepalese velocity model because of the contribution of regional seismic stations at large distances.

Moment tensor inversions are performed over a source depth range of 2 to 30 km in order to test the sensitivity of the approach to depth and to the 3 models. Overall, the focal mechanism is found to be highly consistent, independent of depth and Earth structure. The Lamjung mainshock is described as an almost pure double-couple event (DC=99%) corresponding to a reverse fault earthquake (Fig. 5) with a pair of conjugate fault plane solutions corresponding to steeply dipping thrust / back-thrust faults with strikes, respectively, at 104° and 285° (following Aki and Richards, convention). These strikes obtained by inversion of long period seismic waveforms, correspond roughly to the azimuth of the mountain range, estimated to be N108E between the Annapurna and Langtang ranges. Since the focal mechanism is

almost purely thrust, the coseismic slip is normal to the front of the range.

The inversion-derived seismic moment is found to be  $1.53e+16$  Nm, corresponding to an  $M_w$  of 4.7, and is identical regardless of the velocity model considered here. The depth of the mainshock between 14 and 25 km is more difficult to constrain due to the long wavelengths considered in the moment tensor inversions.

### Comparison of relocation results

#### Comparisons between location approaches

The absolute earthquake locations of the 129 events detected and located within the 14 days following the main Lamjung earthquake of 18 May 2021 define a seismic cluster of 117 events within 10 km of the main rupture zone, regardless of the location method used (see Fig. 6a and b with the HYPO71 solution). The differences between the various solutions are strongly controlled by the degrees of freedom and biases associated with the large primary azimuthal gap, as well as topography and station elevation. Offsets in epicentral locations obtained by the alternative location methods do not exceed the horizontal uncertainty provided by Hypo71. We observe high average residuals of  $0.55 (\pm 0.1)$  seconds for Hypo71 and NonLinLoc. These high residuals may reflect errors in the local velocity model and result in location biases. The average errors on the depths estimated by NonLinLoc are 1 km ( $\pm 0.75$ ) and 2.3 km for Hypo71 (see Laporte (2022) for further details).

At depth, the projection of the seismicity along a N20°E vertical profile (i.e., perpendicular to the front of the high range) shows a cluster of aftershocks above the mainshock hypocenter (Figs. 6 and 7). Whatever the location method used, all aftershock hypocentres are found to be within  $\pm 4$  km of the mainshock. The individual locations of the aftershocks within the cluster vary slightly from one approach to another, but the global spatial distributions are very similar. The HypoDD relative relocations of the aftershocks show a more clustered seismicity, apparently south-dipping (Fig. 7). However, hypoDD relocations appear highly sensitive to the initial absolute location including its potential biases and uncertainties, even after considering only the subset of high quality location events mentioned earlier. We present here one of the HypoDD relative location of the cluster, computed from high quality events, using the initial location computed with Hypo71, a solution that was reasonably convergent and appeared as the best we obtained considering the criteria described in Waldhauser and Ellsworth (2000). 80% of the HypoDD depths are within 5 km of the original depth. The HypoDD relocations appear very sensitive to the initial absolute location. However, whatever the solution, the relative HypoDD locations are on

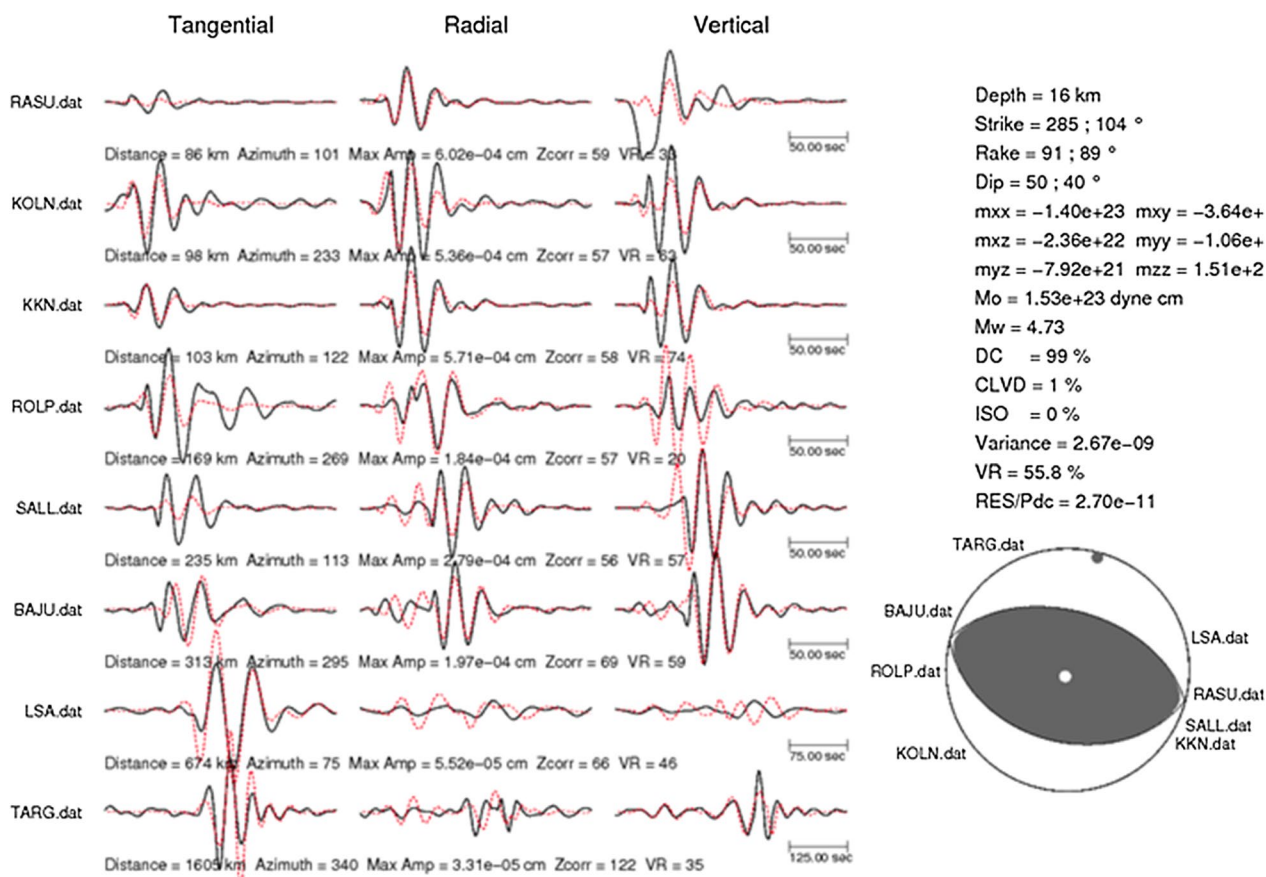


**Fig. 5** Moment tensor solution of the  $M_w$  4.7 ( $M_L$  5.8  $M_{LV}$  5.3) Lamjung mainshock determined using the Time-Domain Deviatoric Moment Tensor Inversion method of Dreger (2003). The observed data (in black) and the synthetic data (in red) calculated using the Earth’s model called CRUST2 show an overall good agreement for the three components of the 8 stations used in the inversion. The solution obtained at 16 km depth indicates a moment magnitude ( $M_w$ ) 4.7 reverse mechanism with nearly pure double-couple (DC) NEE–SWW faulting. Data are filtered between 20 and 40 s period for stations in Nepal, and between 40 and 80 s period for further stations (LSA and TARG)

average found within 1.5 km from the absolute locations previously estimated with Hypo71 and NonLinLoc.

However, note that despite the rather small differences in source depths from one algorithm to another, the current network distribution is probably not optimal for resolving precisely the geometry of the structure that is responsible for the Lamjung seismic activation. In fact, given its magnitude, the size of the source (probably less than 2 km, see discussion below) is smaller than the width of the cluster, regardless of the location method used.

**Insights on depth uncertainties**

Indeed, in order to properly discuss the position of the Lamjung seismic cluster relative to the fault system, as a prerequisite for seismotectonic interpretation, a thorough assessment of the uncertainties and biases associated with the depths determined is crucial to our study. We therefore develop this point below.

The accuracy of the depth estimation mainly relies on the distance of the closest stations, the presence of reliable P- & S-wave picks on these stations, and on the velocity model accuracy (e.g., Gombert et al. 1990; Bondar et al. 2004; Husen and Hardebeck 2010; Gesret et al. 2015; Laporte 2022). It is therefore interesting to take a closer look at the P and S arrivals at the available closest stations. Two stations are less than 10 km from the cluster: station LAMJ at 8–9 km to the western side of the seismicity and the RaspberryShake station S8618 that is about 5–6 km further east. The elevation difference between these two stations is 1250 m while the largest elevation difference between stations reaches 3415 m. Most stations are located to the south-east and south-west of the seismic cluster. The primary azimuthal gap (PAG) is around 125° for the largest events, and up to 140° for the smallest events (Fig. 3B). This PAG is lower than usual for earthquakes under the front of the high topography in Nepal, given the shape of the network

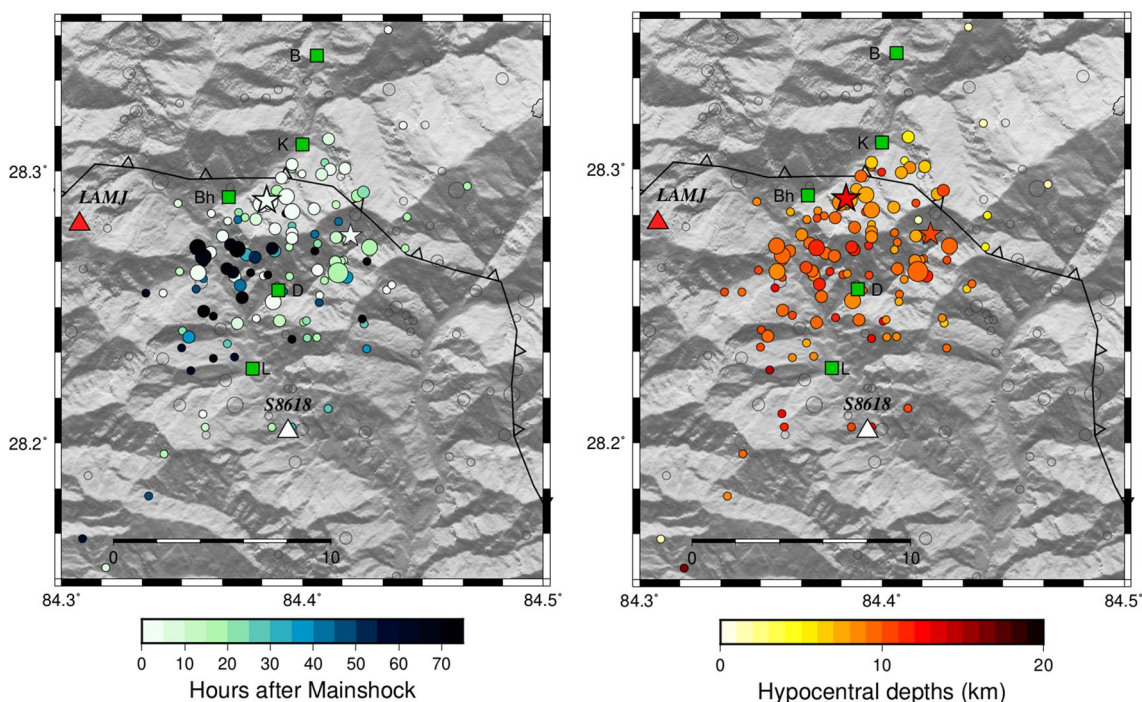


**Fig. 6** Distribution of the seismicity during the Lamjung earthquake crisis (Hypo71 catalogue). The mainshock and largest aftershock epicenters are, respectively, represented by the stars. The green squares locate the villages mentioned in the text (L for Lamjung-Besisahar; D for Deujanthok; Bh for Bhulbule; K for Khuddi; B for Bhaundanda). **A** (Left) Time distribution of the epicenters. **B** (Right) Depth distribution of the hypocentres

and the distribution of the regional seismicity (Adhikari et al. 2021), thanks to the permanent stations recently deployed in the framework of the collaboration with JICA and CEA, as well as thanks to the high density of Seismo@school stations in the area.

Being the only 3-component station within the first 20 km of the cluster, only LAMJ provides optimal S–P depth constraints (see empirical criteria and recommendations listed in Gomberg et al. (1990), Bondar et al. (2004)). 126 pairs of P&S wave arrivals have been detected at this station. Thus we propose to look at S–P delays at station LAMJ to figure out depth uncertainties with regards to firstly, velocity model errors and secondly, epicentral distance uncertainties.

Figure 8 shows the S–P delays determined at station LAMJ. These depend on depth, epicentral distance and the velocity model. Making the approximation that the epicentral locations are well constrained (see next

paragraph), they only depend on the velocity model and earthquake depths. We test four velocity models derived from the velocity model by Pandey (1985) (Fig. 8). First, we take the original model. The S–P delays we obtain for the seismic events at LAMJ, around 1.5 s, suggest that the depths are shallower than the one we obtained previously, for the mainshock (which is likely below the cluster of aftershock, see Discussion section) as well as for the aftershocks, mostly between 4 and 8 km (Fig. 8a). An increase in the model velocities tends to favor even shallower events while a velocity decrease deepens the seismicity (Fig. 8). We also evaluate an “extreme” velocity model, with a decrease of 10% of the velocities and a decrease of 0.05 of the  $V_p/V_s$  ratio (Fig. 8d), bringing the event depths around 14–16 km. Given these results, it is therefore very unlikely that the seismicity could have occurred below, on the lower-shallow dipping segment of the MHT (expected around 20 km). Indeed, to explain an

(See figure on next page.)

**Fig. 7** Seismicity maps and cross sections (black NS line) through the Lamjung seismic cluster. **A, B** using Hypo71 solution plugin Seiscomp; **C, D** using NonLinLoc algorithm; **E, F** with the relative location obtained by HypoDD. The error bars associated with hypocentral positions should not be compared from one method to another, as they represent different measurements and not just residuals. In B–D–F, the origin of the horizontal axis corresponds to the center of the section segments. The stars correspond to the location of the mainshock and the largest aftershock. The beach ball associated with the mainshock was manually translated outside the main cluster to make it easier to see

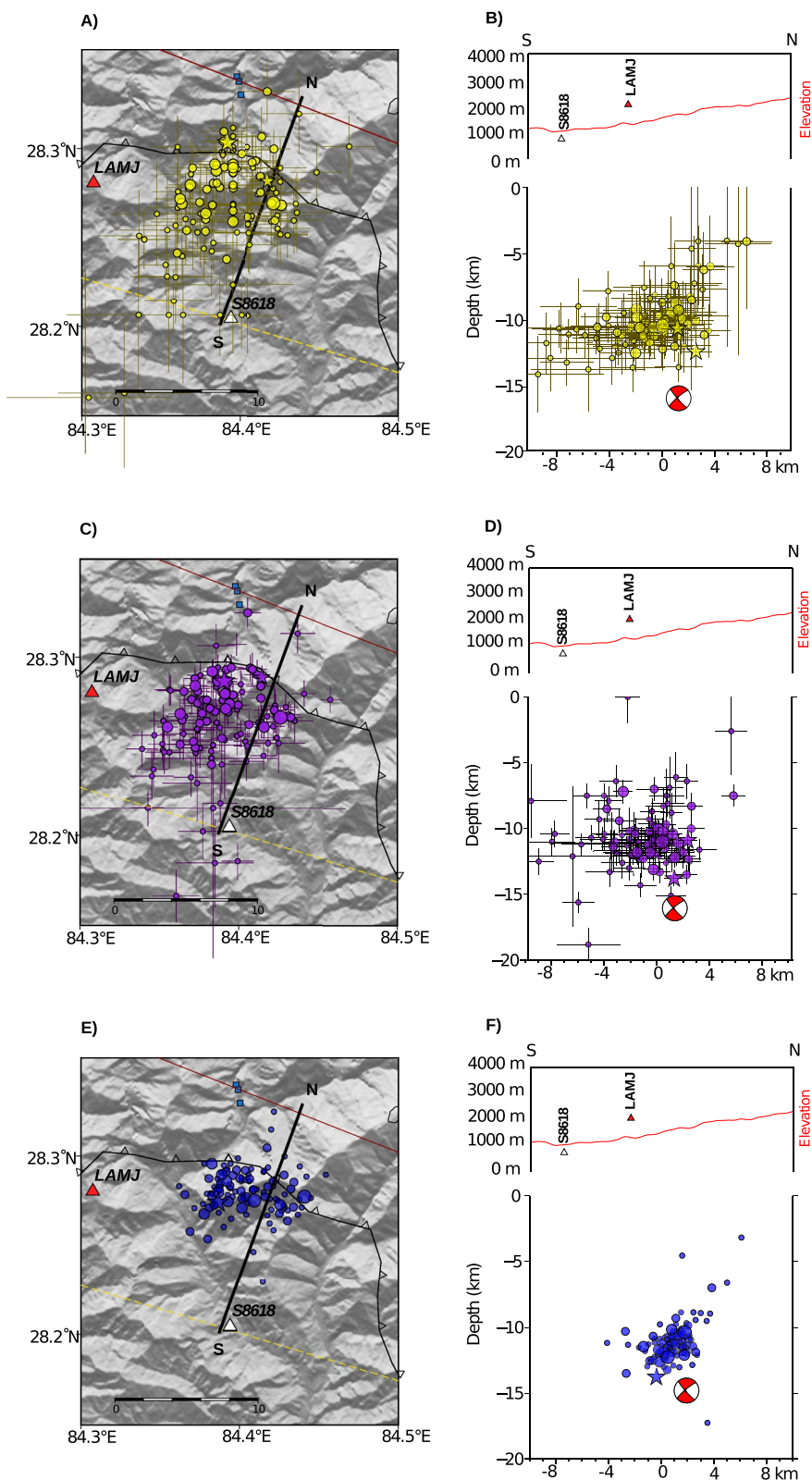
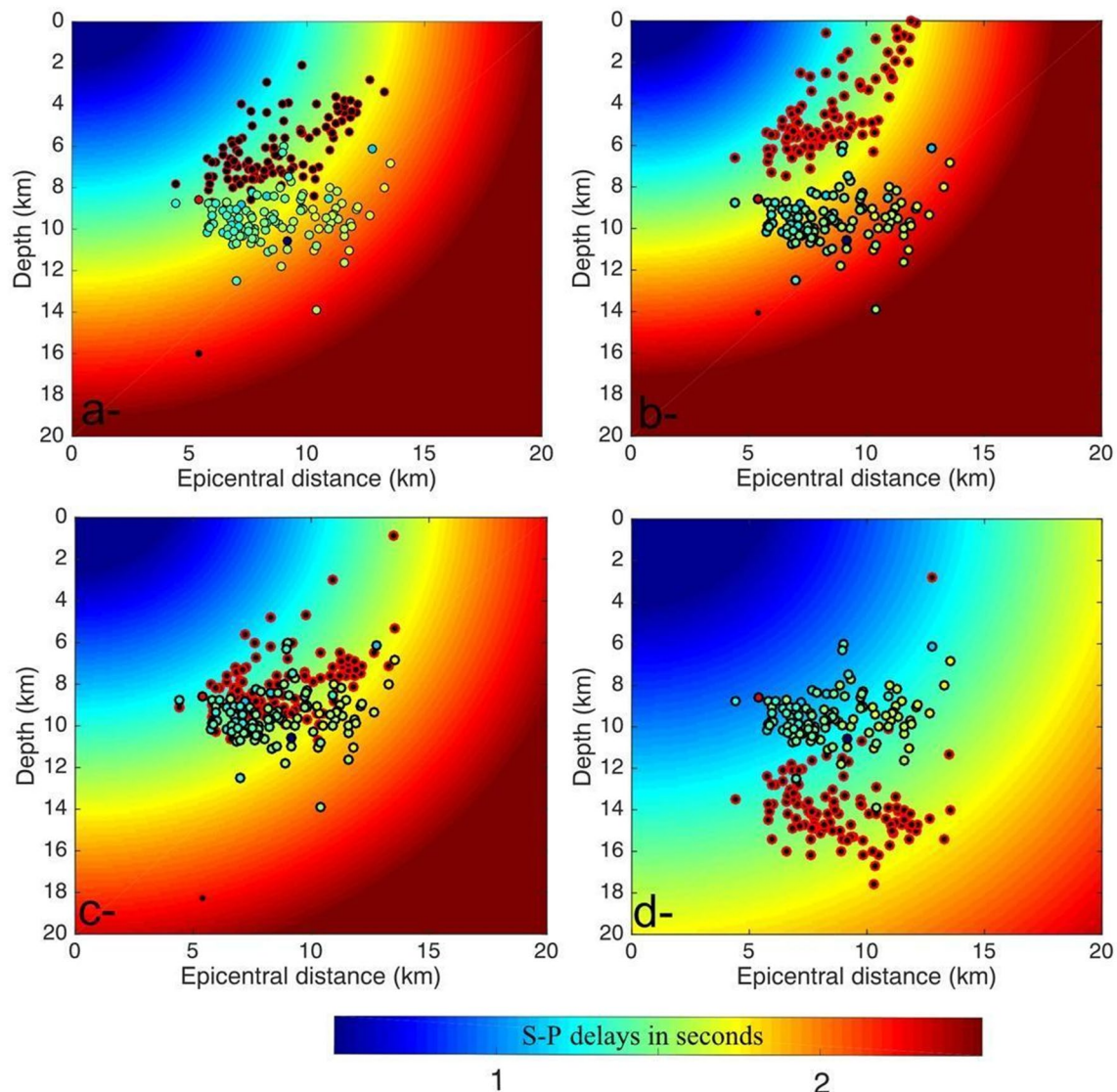


Fig. 7 (See legend on previous page.)



**Fig. 8** Theoretical S-P delays (in seconds, colorscale) for the station LAMJ (Lamjung) according to event epicentral distance and depth, estimated from the Pandey velocity model (a), with a systematic increase of 10% of the P & S wave velocities (b), with a systematic decrease of 10% of the P & S wave velocities (c) and with a systematic decrease of 10% of the velocities and a decrease of the  $V_P/V_S$  ratio from 1.75 (Pandey) to 1.70 (d). Colored dots are estimated event depths and epicentral distances to LAMJ; the color of the dots scale the S-P delays (in seconds) measured by analysts on LAMJ. Red dots show the depths that better fit these measured S-P delays, for the event epicentral distances and for each of the velocity model (a–d)

S-P delay of 1.5 s with an event at 20 km depth, the model velocities have to be divided by a factor 2 or a  $V_P/V_S$  ratio of around 1.4, which is unrealistic. If we assume that the velocity model is correct at  $\pm 10\%$ , then, the events are probably located at a depth of 10 km, in the vicinity of the upper flat of the MHT or even shallower in its hanging wall (see section discussion/interpretation), but could not be associated with the lower flat at depth greater or equal to 20 km.

An error in the epicentral distance estimation could also have an impact on the S-P delays by decreasing the depth estimation if the source–station distance is larger than estimated whereas it would increase the depth for closest distances. More precisely, it would shift the events to the left on Fig. 8. However, it is unlikely that the distance is less than 4–5 km, given that all the P-phase arrivals are first detected at station S8618. They are then observed at station LAMJ, which is 12 km away from station S8618. Hence, in any 1D layered velocity structure,

the minimum epicentral distance between LAMJ and any event is 6 km (at the exact middle point between LAMJ and S8618). Assuming a 3D velocity structure and extreme high velocities in the vicinity of S8618, being 2 times the velocities around LAMJ, the minimum distance reaches 4 km between LAMJ and the seismicity. Therefore, it is very unlikely that the seismicity is located closer than 1–2 km from station LAMJ. It could be argued that this has a limited effect on depth estimation. On the contrary, one could easily imagine that the seismicity is further away from the stations, within a cluster a few kilometers to the north. Such a case would favor shallower events given the LAMJ S-P delays.

Based on these tests, we argue that the Lamjung seismic cluster is located at depths between 5 and 15 km for almost all the aftershocks. This is consistent with the depths obtained by all three locators.

### Interpretations and discussion

The epicenters of the mainshock and the best-located aftershocks are restricted to an area of  $\sim 10 \times 10$  km, between the town of Besisahar-Lamjung and the village of Deujanthok in the south, and the village of Kudi in the north (Fig. 6). This aftershock region is significantly larger than the typical area ruptured by an  $M_w$  4.7 earthquake, given empirical laws relating moment magnitude and the length of the subsurface rupture (Wells and Coppersmith 1994). Indeed, an  $M_w$  4.8 earthquake (the lower bound of the magnitudes considered for the regression in the empirical dataset) is associated with an average length of subsurface reverse rupture of less than 2 km, and a surface rupture of less than 4 km<sup>2</sup>.

The fault patch that ruptured during the Lamjung earthquake and subsequent aftershocks lies at mid-crustal depths (between 10 and 15 km for the mainshock and 5–15 for most aftershocks) in the vicinity of the MHT upper flat/decollement that was imaged a few tens of kilometers to the east below the HiClimb experiment (Nabelek et al. 2009; Duputel et al. 2016). It is also consistent with the depth range at which the 2015  $M_w$  7.9 Gorkha earthquake nucleated (e.g., Grandin et al. 2015; Engdahl et al. 2020), below the town of Barpak, about 30 km to the east in a similar structural position relative to the Main Central Thrust (MCT) trace and the high topography (see Fig. 2). The Lamjung earthquake and aftershocks occurred at the transition between a region of slow uplift to the south and a region of rapid uplift and incision to the north (e.g., Hodges et al. 2004; Blythe et al. 2007; Whipp et al. 2007). It is often recognized as coinciding with the upper flat–ramp transition of the MHT, with the flat–ramp–flat plate boundary thrust accommodating most of the deformation between India plate and the Himalayas (e.g., Cattin and Avouac 2000; Lavé

and Avouac 2001). In addition, several imbricate slivers of Lesser Himalayan rocks have been mapped below the MCT and are considered to compose a Lesser Himalayan duplex (e.g., Robinson and Martin 2014; Khanal 2014; Ghoshal et al. 2023).

The steep planes of the focal mechanism of the Lamjung earthquake (either 40°N or 50°S) are inconsistent with a rupture of a flat or shallow northward dipping thrust (Fig. 5). The earthquake is therefore unlikely associated with the rupture of the MHT upper decollement, and certainly not with the rupture of the lower flat, which is given at larger depths (around 20 km at its shallowest) and significantly farther north (e.g., Hubbard et al. 2016; Wolff et al. 2022; Ghoshal et al. 2023). The earthquake is also unlikely associated to a rupture in the footwall of the MHT, in the India Plate, given the depths we obtained. However, it could be related with (1) a rupture of a segment of the main active ramp of the flat–ramp–flat, or (2) a rupture of a backthrust, similarly to what was proposed for the Sarshin earthquake in 1997 or for the north Karnali earthquake in December 2015 (Hoste-Colomer et al. 2017; Laporte et al. 2021), or (3) with the activation of an out-of-sequence thrust, related to internal deformation of the antiformal stack (Baillard et al. 2017; Mendoza et al. 2019), or even (4) with a more significant out-of-sequence (“splay fault”) below the MCT (Hodges et al. 2004).

The trace of the physiographic transition PT2, considered by Hodges et al. (2004) as an active out-of-sequence thrust develops above the Lamjung, 2021 seismic cluster. Given its dip, the associated fault plane at depth falls 5 km above the Lamjung epicenter and is therefore too shallow to be a good candidate to be associated with the seismic cluster. The association with a backthrust is unlikely. Indeed, the dip of the geological units (mainly thick Quartzites) above the Lamjung earthquake and up to the MCT zone is monoclinial, dipping about 30°N, interpreted as a sliver above the northern edge of the antiformal stack of the Lesser Himalayan duplex (Khanal 2014; Ghoshal et al. 2023), a tectonic setting never associated with a backthrust structure. Contrary to the tectonic setting of the 1997 Sarshin earthquake or the 2015 north Karnali earthquake (Hoste-Colomer et al. 2017; Laporte et al. 2021), the seismicity here develops at depths similar not to the lower but to the upper decollement of the flat–ramp–flat tectonic system. The activation of a steep backthrust, branching on a low friction flat thrust fault, is more unlikely than at the toe of a steep mid-crustal ramp, where local shear zones within the hinge above the low flat/ramp are predicted by mechanical models (e.g., Souloumiac et al. 2009). As mentioned above in the list of possible scenarios, another option is to see the seismic cluster associated to a rupture at the contact between two

slivers of the mid-crustal duplex, a scenario previously documented elsewhere in Nepal (Baillard et al. 2017; Hoste-Colomer et al. 2018; Laporte et al. 2021). This scenario cannot be rejected but cannot be proven either given the uncertainties associated with the geometry of local secondary tectonic structures at depth often best constrained by balanced cross sections extrapolated from the surface geology (Khanal 2014; Ghoshal et al. 2023)—but which are also uncertain because it is inferred outside the scope of the balanced-cross-section assumptions. Our preferred interpretation is therefore the one that appears to be related to the simplest scenario involving a partial rupture of the mid-crustal ramp. The precise location of the mid-crustal ramp in this area is rather elusive because it has never been imaged by local geophysical experiments. However, this ramp is needed to connect the upper decollement to the lower decollement of the MHT fault. It is also consistent with the local state of stress at the toe of the high topography. It is finally consistent with the long-term thermokinematic evolution of the Lesser Himalayas, their stacking, their fast exhumation at the toe of the high range, and the construction of the principal Lesser Himalayan antiform. One of the balanced cross sections equilibrated in the area (Ghoshal et al. 2023) suggests, on the basis of the geology and of the quaternary exhumation rates, that the mid-crustal

ramp develops 10–15 km to the north of the seismicity cluster. However, the west-central region of Nepal, and in particular the Marsyangdi River region along which geomorphic studies have been documented, is also known to be associated with rates of rapid modern/Holocene uplift located well south of the high range (Lavé and Avouac 2001; Grandin et al. 2012). Grandin et al. (2012) suggests that this uplift pattern is related to the recent (Holocene) abandonment of the mid-crustal ramp below the high range, for a ramp 10–15 km southward. The seismic activity at mid-crustal depths, associated to a steep fault plane solution could therefore possibly be associated with the activation of the updip end of the ramp. This would be consistent with our observations showing that the mainshock happened at slightly greater depths and northward relative to the postseismic cluster.

At the scale of the cluster (10×10 km), the seismicity from the Hypo71 solution appears to slightly migrate toward the southwest after two days (see Fig. 6A). However, this possible migration is not confirmed by the HypoDD relocation solutions. We therefore estimate that this possible migration of the seismic activity is not resolved sufficiently well for interpretation (Fig. 9).

The simultaneity of the seismicity at the western edge of the Gorkha earthquake rupture and in the Lamjung region was also questioned. Indeed, a first cluster of

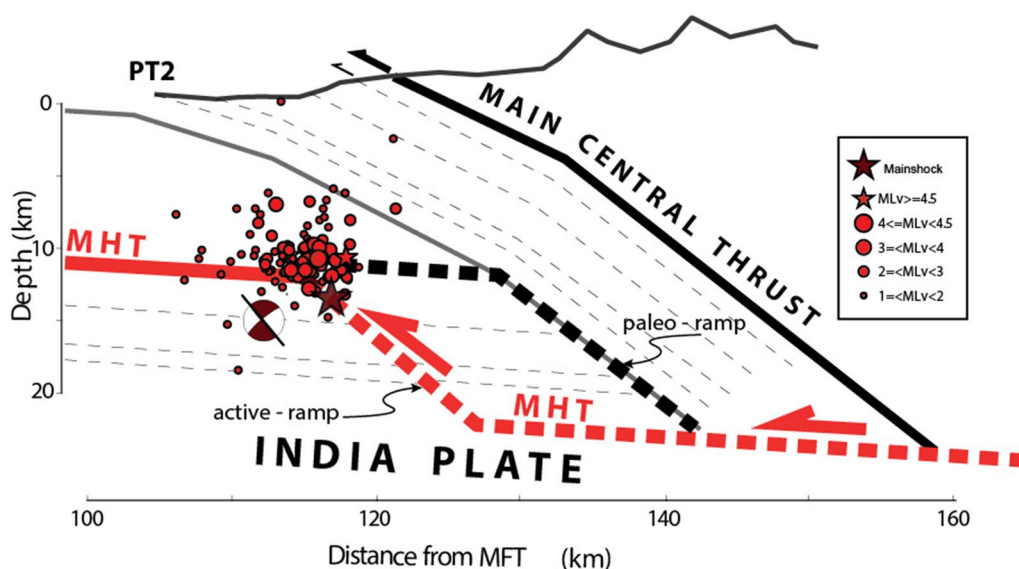


**Fig. 9** Seismotectonic interpretation of the seismicity (NonLinLoc catalogue, the figure with Hypo71 results is only marginally different) during the Lamjung earthquake crisis. The mainshock and largest aftershock epicenters are, respectively, represented by the dark red and red stars. The structures are constrained by field observations (structural measures of the bedding and schistosity) measured locally, that complemented a previous cross section built further east in Adhikari et al. (2021) as well as the balanced cross section of Ghoshal et al. 2023. The main difference with the recently published Ghoshal et al. 2023 cross section—optimized using Plio-Quaternary low-temperature chronometry ages—is that the mid-crustal ramp presented here as active is consistent with a very recent Holocene migration of the ramp documented by Grandin et al. (2012) and the location of the Physiographic Transition 2 (PT2), which marks the southern extent of a narrow region of high incision and exhumation

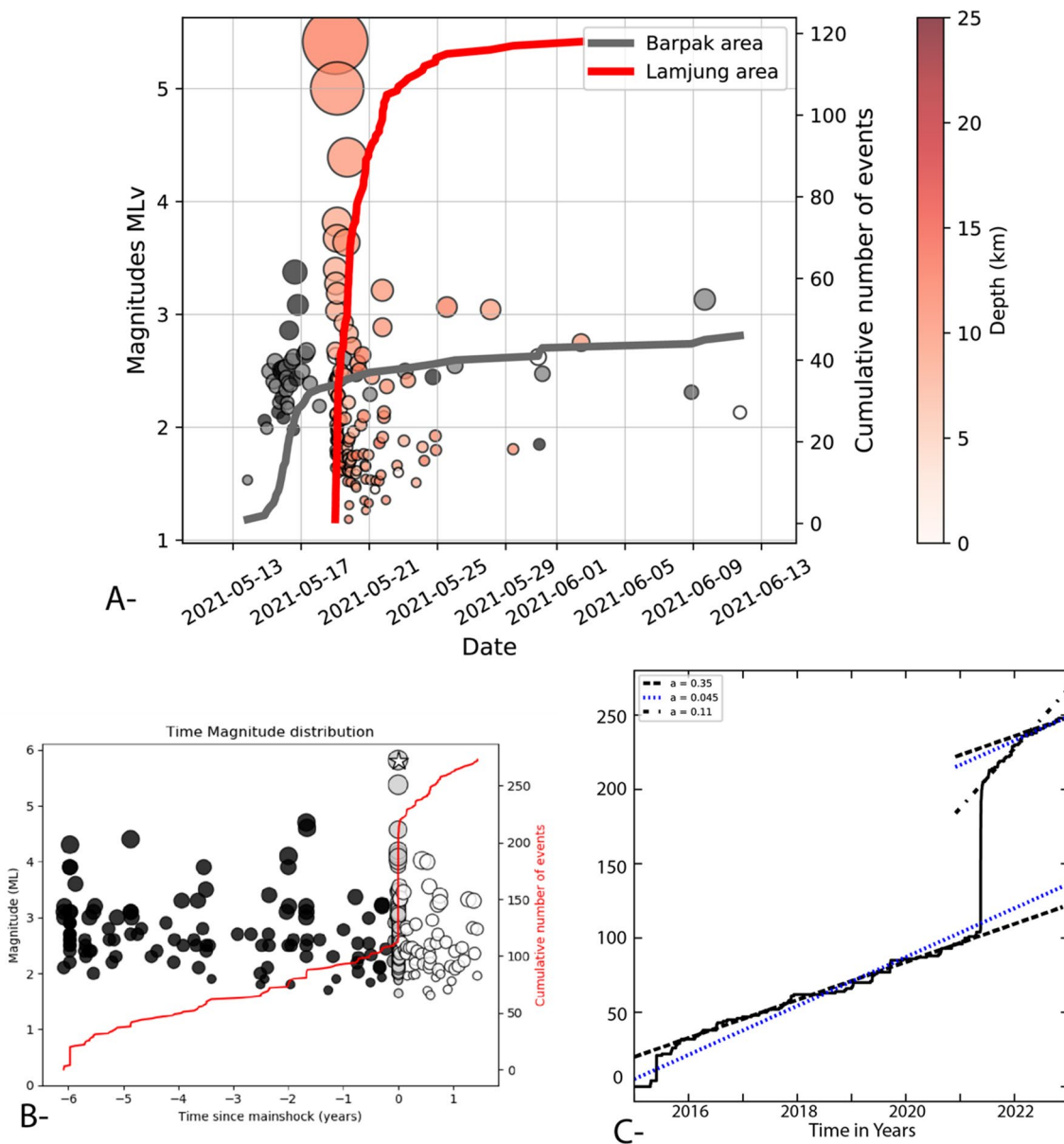


**Fig. 10** (A Top) Seismicity and cumulative number of earthquakes detected in Barpak (grey 28.0–28.2N 84.7–84.9E) and Lamjung area (red 28.15–28.355N 84.3–84.5E) in May–June 2021. (B Bottom left): seismicity and cumulative number of earthquakes detected in Lamjung area (as a function of the time in hours since the mainshock). (C Bottom right): cumulative number of events in Lamjung area above  $M_c 2.0$ —2015–2022—The seismicity rate before 2021 is represented by the dashed-line and has a value of 0.035. In 2021, the seismicity rate is 0.11 (dash-dotted line) and decreases to 0.045 in 2022 (dashed line)

seismicity happened a few hours prior to the occurrence of the Lamjung crisis, less than 30 km eastward (see Figs. 2 and 10A). However, despite a careful look at potential earthquake migrations from the Gorkha earthquake main ruptured trace to Lamjung, we were not able to demonstrate a causal relation between both earthquake clusters.

The cumulative number of events follows a trend of a typical mainshock–aftershock sequence with a high seismic rate during the first hours after the mainshock and a progressive decay as a function of time, with a visible decay during the two weeks following the mainshock (Fig. 10). The time–magnitude distribution shows as well a decay of magnitudes over time consistent with a mainshock–aftershock sequence (Fig. 10). The main

aftershock of  $M_L$  5.3  $M_{L_v}$  5.0 occurred two and a half hours after the main event and two other aftershocks of magnitude  $M_{L_v}$  above 3.5 occurred within 17 h.

### Conclusions, implications and perspectives

The 2021  $M_L$  5.8 Lamjung earthquake occurred in central western Nepal, 30 km west of the Barpak epicenter of the Gorkha earthquake, and at an even closer to the fault plane ruptured by the 2015  $M_w$  7.9 Gorkha earthquake. It is the largest earthquake recorded in this area in the last 40 years. The earthquake was followed by more than 120 aftershocks located within 10 km of the mainshock. The earthquake ruptured a steep (dip of about 40°), kilometer-long fault plane at the updip end of the mid-crustal ramp of the Main Himalayan Thrust. The flat/decollement of the fault system further south is considered to be fully locked (e.g., Ader et al. 2012; Lindsey et al. 2018; Dal Zilio et al. 2020; Michel et al. 2021). Based on current knowledge of the historical earthquakes that occurred in the region, this segment of the MHT, south of the Gorkha rupture (Fig. 1), has not been ruptured since the 1505 and/or 1344 AD earthquakes, ascertaining a large slip deficit accumulated in the area, assuming that the system remains fully locked between large earthquakes. The slip deficit since then can therefore reach and even exceed 10 to 14 m and is therefore associated with a very high seismogenic potential, given the lateral extension of the fault segment remaining unruptured along strike since medieval times (Bollinger et al. 2016).

The location of the Lamjung cluster, close to the western edge of the post-2015 earthquake afterslip zone, 30 km west of the hypocenter of the Gorkha earthquake, in a similar structural position, led us to suspect an intriguing westward spread of seismic activity. Fortunately, the seismic rate decreased within a few days, with the earthquake rate gradually reducing to the pre-Lamjung cluster microearthquake production rate after one month (Fig. 10). Furthermore, the earthquake rate is now back to pre-Gorkha earthquake rate in the area (Fig. 10b, c), despite the still high activity rate of aftershock in the trace of the 2015 rupture, an activity believed to remain higher than the interseismic rate during another 5 years at least (Adhikari et al. 2023). We did not notice any resolvable signs of migration of the microseismicity over the long term at the scale of the northwestern edge of the rupture. However, seismic activity at the western edge of the ruptured zone in 2015 leads us to further monitor the area very carefully.

### Acknowledgements

We acknowledge the Nepal–Japan collaboration supported by the SATREPS program of JICA/JST, Japan and Li Li CEA project, China, respectively, for access to the waveforms of the seismic stations deployed in collaboration with DMG by Japan International Collaboration Agency and China Earthquake Administration. We thank György Hetényi for initiating the Seismo@School project as

part of Shiba Subedi's Ph.D. thesis, for making the data available online, and for discussions on Marine Laporte's early relocation and this paper. The authors are also most grateful to Monika Jha, chief of NEMRC and Sudhir Rajaur, former director general of DMG, who facilitated the work as well as to all the staff of the DMG and DASE who contributed indirectly to the maintenance of the stations of the national seismological network. We thank Remi Bossu for access to felt reports archived at CSEM and Deujanthok Ward officer for his testimonies and Lamjung district police office for the access to the list of reported damages. We thank the two anonymous reviewers and the editor K. Koketsu for their comments, which improved the manuscript.

### Author contributions

BK, section chief of Earthquake Monitoring and Hazard Evaluation section at NEMRC, initiated this study. With MB and LBA, he revised the seismic alerts published after the mainshock and largest aftershocks, picked the local phases and generated the first bulletin of earthquakes. ML, DB and NWW worked on the relocation and the production of the main figures of the article. ML also studied the earthquake at teleseismic distance, see her Phd thesis (Laporte 2022). JLT and AT provided, respectively, contributions including results and expertise on the quality of the hypocentral location, and on the moment tensor inversion. LB coordinated the research work and drafted the manuscript. All authors read, amended and approved the final manuscript.

### Funding

This research was done in the framework of the collaboration between the Department of Mines and Geology (DMG), Nepal and Département Analyse Surveillance Environnement (DASE), France, and funded by both institutes.

### Availability of data and materials

Data available upon request to koirala\_bharat@yahoo.com.

### Declarations

### Competing interests

The authors declare that they have no competing interests.

### Author details

<sup>1</sup>Department of Mines and Geology, National Earthquake Monitoring and Research Center, Kathmandu, Nepal. <sup>2</sup>CEA, DIF, 91297 Arpajon, France. <sup>3</sup>IRAP, UMR 5277, Université de Toulouse, CNRS, CNES, UPS (Toulouse), Toulouse, France. <sup>4</sup>Institute of Earth Sciences, Faculty of Geosciences and Environment, University of Lausanne, Lausanne, Switzerland.

Received: 23 March 2023 Accepted: 24 August 2023

Published online: 18 October 2023

### References

- Ader T, Avouac JP, Liu-Zeng J, Lyon-Caen H, Bollinger L, Galetzka J, Flouzat M (2012) Convergence rate across the Nepal Himalaya and interseismic coupling on the Main Himalayan Thrust: implications for seismic hazard. *J Geophys Res-Solid*. <https://doi.org/10.1029/2011JB009071>
- Adhikari LB, Gautam UP, Koirala B, Bhattarai M, Kandel T, Gupta RM, Timsina C, Maharjan N, Maharjan K, Dahal T, Hoste-Colomer R, Cano Y, Dandine M, Guilhem A, Merrer S, Roudil P, Bollinger L (2015) The aftershock sequence of the April 25 2015 Gorkha-Nepal earthquake. *Geophys J Int* 203:2119–2124
- Adhikari LB, Bollinger L, Vergne J, Lambotte S, Chanard K, Laporte M, Perrier F (2021) Orogenic collapse and stress adjustments revealed by an intense seismic swarm following the 2015 Gorkha earthquake in Nepal. *Front Earth Sci*. <https://doi.org/10.3389/feart.2021.659937>
- Adhikari LB, Laporte M, Bollinger L, Vergne J, Lambotte S, Koirala BP, Perrier F (2023) Seismically active structures of the Main Himalayan Thrust revealed before, during and after the 2015 Mw 7.9 Gorkha earthquake in Nepal. *Geophys J Int* 232(1):451–471
- Argand E (1922) La tectonique de l'Asie. Conférence faite à Bruxelles, le 10 août 1922. In: *Congrès géologique international (XIIIe session)-Belgique 1922*: 171–372

- Avouac JP (2003) Mountain building, erosion, and the seismic cycle in the Nepal Himalaya. *Adv Geophys* 46:1–80
- Avouac JP, Meng L, Wei S, Wang T, Ampuero JP (2015) Lower edge of locked main Himalayan thrust unzipped by the 2015 Gorkha earthquake. *Nat Geosci* 8(9):708–711
- Bai L, Klemperer SL, Mori J, Karplus MS, Ding L, Liu H, Li G, Song B, Dhakal S (2019) Lateral variation of the main Himalayan thrust controls the rupture length of the 2015 Gorkha earthquake in Nepal. *Sci Adv* 5(6):eaav0723
- Baillard C, Lyon-Caen H, Bollinger L, Rietbrock A, Letort J, Adhikari LB (2017) Automatic analysis of the Gorkha earthquake aftershock sequence: evidences of structurally segmented seismicity. *Geophys J Int* 209(2):1111–1125
- Bassin C, Laske G, Masters G (2000) The current limits of resolution for surface wave tomography in North America. *EOS Trans AGU* 81:F897
- Bilham R (2019) Himalayan earthquakes: a review of historical seismicity and early 21st century slip potential. *Geol Soc Spec Publ* 483(1):423–482
- Blythe AE, Burbank DW, Carter A, Schmidt K, Putkonen J (2007) Plio-quaternary exhumation history of the central Nepalese Himalaya: 1. Apatite and zircon fission track and apatite [U-Th]/He analyses. *Tectonics*. <https://doi.org/10.1029/2006TC001990>
- Bollinger L, Avouac JP, Cattin R, Pandey MR (2004) Stress buildup in the Himalaya. *J Geophys Res* 109:B11405. <https://doi.org/10.1029/2003JB002911>
- Bollinger L, Tapponnier P, Sapkota SN, Klinger Y (2016) Slip deficit in central Nepal: omen for a repeat of the 1344 AD earthquake? *Earth Planet Space* 68(1):1–12. <https://doi.org/10.1186/s40623-016-0389-1>
- Bondar I, Myers SC, Engdahl ER (2004) Epicentre accuracy based on seismic network criteria. *Geophys J Int* 156(3):483–496
- Cattin R, Avouac JP (2000) Modeling mountain building and the seismic cycle in the Himalaya of Nepal. *J Geophys Res* 105:13389–13407. <https://doi.org/10.1029/2000JB900032>
- Cattin R, Martelet G, Henry P, Avouac JP, Diament M, Shakya TR (2001) Gravity anomalies, crustal structure and thermo-mechanical support of the Himalaya of Central Nepal. *Geophys J Int* 147(2):381–392
- Dal Zilio L, Jolivet R, van Dinther Y (2020) Segmentation of the Main Himalayan Thrust illuminated by Bayesian inference of interseismic coupling. *Geophys Res Lett* 47(4):e2019GL086424
- Dal Zilio L, Hetenyi G, Hubbard J, Bollinger L (2021) Building the Himalaya from tectonic to earthquake scales. *Nat Rev*. <https://doi.org/10.1038/s43017-021-00143-1>
- Dreger D (2003) 85.11 TDMT\_INV: time domain seismic moment tensor INVersion. *Int Geophys* 81:1627–1627. [https://doi.org/10.1016/S0074-6142\(03\)80290-5](https://doi.org/10.1016/S0074-6142(03)80290-5)
- Duputel Z, Vergne J, Rivera L, Wittlinger G, Farra V, Hetényi G (2016) The 2015 Gorkha earthquake: a large event illuminating the Main Himalayan Thrust fault. *Geophys Res Lett* 43(6):2517–2525
- Duverger C, Mazet-Roux G, Bollinger L, Guilhem Trilla A, Vallage A, Hernandez B, Cansi Y (2021) A decade of seismicity in metropolitan France (2010–2019): the CEA/LDG methodologies and observations. *BSGF Earth Sci Bull* 192:25. <https://doi.org/10.1051/bsgf/2021014>
- Engdahl ER, Di Giacomo D, Sakarya B, Gkarlaoui CG, Harris J, Storchak DA (2020) ISC-EHB 1964–2016, an improved data set for studies of earth structure and global seismicity. *Astr Soc P* 7(1):e2019EA000897. <https://doi.org/10.1029/2019EA000897>
- Font Y, Kao H, Lallemand S, Liu CS, Chiao LY (2004) Hypocentre determination offshore of eastern Taiwan using the Maximum Intersection method. *Geophys J Int* 158(2):655–675. <https://doi.org/10.1111/j.1365-246X.2004.02317.x>
- Gesret A, Desassis N, Noble M, Romary T, Maisons C (2015) Propagation of the velocity model uncertainties to the seismic event location. *Geophys J Int* 200(1):52–66
- Ghoshal S, McQuarrie N, Huntington KW, Robinson DM, Ehlers TA (2023) Testing erosional and kinematic drivers of exhumation in the central Himalaya. *Earth Planet Sci Lett* 609:118087. <https://doi.org/10.1016/j.epsl.2023.118087>
- Gomberg JS, Shedlock KM, Roecker SW (1990) The effect of S-wave arrival times on the accuracy of hypocenter estimation. *B Seismol Soc Am* 80(6A):1605–1628
- Grandin R, Doin MP, Bollinger L, Pinel-Puysegur B, Ducret G, Jolivet R, Sapkota SN (2012) Long-term growth of the Himalaya inferred from interseismic InSAR measurement. *Geology* 40(12):1059–1062
- Grandin R, Vallée M, Satriano C, Lacassin R, Klinger Y, Simoes M, Bollinger L (2015) Rupture process of the Mw= 7.9 2015 Gorkha earthquake (Nepal): insights into Himalayan megathrust segmentation. *Geophys Res Lett* 42(20):8373–8382
- Hauck ML, Nelson KD, Brown LD, Zhao W, Ross AR (1998) Crustal structure of the Himalayan orogen at ~ 90° east longitude from Project INDEPTH deep reflection profiles. *Tectonics* 17(4):481–500. <https://doi.org/10.1029/98TC01314>
- He P, Lei J, Yuan X, Xu X, Xu Q, Liu Z, Zhou L (2018) Lateral Moho variations and the geometry of the Main Himalayan thrust beneath the Nepal Himalayan orogen revealed by teleseismic receiver functions. *Geophys J Int* 214(2):1004–1017
- Herrmann RB (2013) Computer programs in seismology: an evolving tool for instruction and research. *Seismol Res Lett* 84(6):1081–1088. <https://doi.org/10.1785/0220110096>
- Hodges KV, Wobus C, Ruhl K, Schildgen T, Whipple K (2004) Quaternary deformation, river steepening, and heavy precipitation at the front of the Higher Himalayan ranges. *Earth Planet Sci Lett* 220(3–4):379–389. [https://doi.org/10.1016/S0012-821X\(04\)00063-9](https://doi.org/10.1016/S0012-821X(04)00063-9)
- Hoste-Colomer R, Bollinger L, Lyon-Caen H, Burtin A, Adhikari LB (2017) Lateral structure variations and transient swarm revealed by seismicity along the Main Himalayan Thrust north of Kathmandu. *Tectonophysics* 714:107–116
- Hoste-Colomer R, Bollinger L, Lyon-Caen H, Adhikari LB, Baillard C, Benoit A et al (2018) Lateral variations of the midcrustal seismicity in Western Nepal: seismotectonic implications. *Earth Planet Sci Lett* 504:115–125. <https://doi.org/10.1016/j.epsl.2018.09.041>
- Hubbard J, Almeida R, Foster A, Sapkota SN, Bürgi P, Tapponnier P (2016) Structural segmentation controlled the 2015 Mw 7.8 Gorkha earthquake rupture in Nepal. *Geology* 44(8):639–642
- Husen S, Hardebeck J (2010) Earthquake location accuracy, CORSSA Ingleby T, Wright TJ, Hooper A, Craig TJ, Elliott JR (2020) Constraints on the geometry and frictional properties of the Main Himalayan Thrust using coseismic, postseismic, and interseismic deformation in Nepal. *J Geophys Res-Solid* 125(2):e2019JB019201
- Khanal S (2014) Structural and kinematic evolution of the Himalayan thrust belt, central Nepal [Ph.D. thesis]: Tuscaloosa, University of Alabama. pp. 1–185.
- Laporte M, Bollinger L, Lyon-Caen H, Hoste-Colomer R, Duverger C, Letort J, Riesner M, Koirala BP, Bhattarai M, Kandel T, Timsina C, Adhikari LB (2021) Seismicity in far western Nepal reveals flats and ramps along the Main Himalayan Thrust. *Geophys J Int*. <https://doi.org/10.1093/gji/ggab159>
- Laporte M (2022) Contribution à l'amélioration de l'estimation de la profondeur hypocentrale à partir de réseaux régionaux ou globaux, Unpublished PhD thesis, ENS-PSL
- Laske G, Masters G, Ma Z, Pasyanos M (2013) Update on CRUST1.0-A 1-degree Global Model of Earth's Crust, *Geophys Res Abstracts*, 15, Abstract EGU2013-2658
- Lavé J, Avouac JP (2001) Fluvial incision and tectonic uplift across the Himalayas of central Nepal. *J Geophys Res-Solid* 106(B11):26561–26591
- Lee WHK, Lahr JC (1972) HYPO71: a computer program for determining hypocenter, magnitude, and first motion pattern of local earthquakes. US Department of the Interior, Geological Survey, National Center for Earthquake Research. pp 1–100
- Letort J, Bollinger L, Lyon-Caen H, Guilhem A, Cano Y, Baillard C, Adhikari LB (2016) Teleseismic depth estimation of the 2015 Gorkha–Nepal aftershocks. *Geophys J Int* 207(3):1584–1595
- Lindsey EO, Almeida R, Mallick R, Hubbard J, Bradley K, Tsang LL, Hill EM (2018) Structural control on downslip locking extent of the Himalayan megathrust. *J Geophys Res-Solid* 123(6):5265–5278
- Lomax A, Virieux J, Volant P, Berge-Thierry C (2000) Probabilistic earthquake location in 3D and layered models: Introduction of a Metropolis-Gibbs method and comparison with linear locations. In: Thurber CH, Rabinowitz N (eds) *Advances in seismic event location*. Springer, Berlin, pp 101–134
- Lomax A, Michelini A, Curtis A (2009) Earthquake location, direct, global-search methods. In: Meyers RA (ed) *Encyclopedia of complexity and systems science*. Springer, Berlin, pp 2449–2473
- Mendoza MM, Ghosh A, Karplus MS, Klemperer SL, Sapkota SN, Adhikari LB, Velasco A (2019) Duplex in the Main Himalayan Thrust illuminated by aftershocks of the 2015 Mw 7.8 Gorkha earthquake. *Nat Geosci* 12(12):1018–1022

- Michel S, Jolivet R, Rollins C, Jara J, Dal Zilio L (2021) Seismogenic potential of the Main Himalayan Thrust constrained by coupling segmentation and earthquake scaling. *Geophys Res Lett* 48(13):e2021GL093106
- Nábělek J, Hetényi G, Vergne J, Sapkota S, Kafle B, Jiang M, Team THC (2009) Underplating in the Himalaya-Tibet collision zone revealed by the Hi-CLIMB experiment. *Science* 325(5946):1371–1374
- Nakaya S (2006) Spatiotemporal variation in b value within the subducting slab prior to the 2003 Tokachi-oki earthquake (M 8.0), Japan. *J Geophys Res-Solid*. <https://doi.org/10.1029/2005JB003658>
- Pandey MR (1985) Seismic model of central and eastern lesser Himalaya of Nepal. *J Nepal Geol Soc* 3:1–11
- Pandey MR, Tandukar RP, Avouac JP, Lave J, Massot JP (1995) Interseismic strain accumulation on the Himalayan crustal ramp (Nepal). *Geophys Res Lett* 22(7):751–754
- Richter CF (1935) An instrumental earthquake magnitude scale. *B Seismol Soc Am* 25(1):1–32
- Ritzwoller MH, Shapiro NM, Barmin MP, Levshin AL (2002) Global surface wave diffraction tomography. *J Geophys Res Solid Earth* 107(B12):E5E-4
- Robinson DM, Martin AJ (2014) Reconstructing the greater Indian margin: a balanced cross section in central Nepal focusing on the Lesser Himalayan duplex. *Tectonics* 33(11):2143–2168. <https://doi.org/10.1002/2014TC003564>
- Scholz CH (2015) On the stress dependence of the earthquake b value. *Geophys Res Lett* 42(5):1399–1402
- Schulte-Pelkum V, Monsalve G, Sheehan A, Pandey MR, Sapkota S, Bilham R, Wu F (2005) Imaging the Indian subcontinent beneath the Himalaya. *Nature* 435(7046):1222–1225
- Souloumiac P, Leroy YM, Maillot B, Krabbenhoft K (2009) Predicting stress distributions in fold-and-thrust belts and accretionary wedges by optimization. *J Geophys Res* 114:B09404. <https://doi.org/10.1029/2008JB005986>
- Subedi S, Hetényi G, Denton P, Sauron A (2020a) Seismology at school in Nepal: a program for educational and citizen seismology through a low-cost seismic network. *Front Earth Sci* 8:73
- Subedi S, Hetényi G, Shackleton R (2020b) Impact of an educational program on earthquake awareness and preparedness in Nepal. *Geosci Comm* 3(2):279–290
- Tarantola A, Valette B (1982) Generalized nonlinear inverse problems solved using the least squares criterion. *Rev Geophys* 20(2):219–232
- Upreti BN (1999) An overview of the stratigraphy and tectonics of the Nepal Himalaya. *J Asian Earth Sci* 17(5–6):577–606
- Waldhauser F, Ellsworth WL (2000) A double-difference earthquake location algorithm: method and application to the northern Hayward fault, California. *B Seismol Soc Am* 90(6):1353–1368
- Weber B, Becker J, Hanka W, Heinloo A, Hoffmann M, Kraft T, Pahlke D, Reinhardt J, Saul J, Thoms H (2007) Seiscomp3—Automatic and interactive real time data processing, EGU General Assembly Conference Abstracts, Vienna, Austria, April 2007.
- Wells DL, Coppersmith KJ (1994) New empirical relationships among magnitude, rupture length, rupture width, rupture area, and surface displacement. *B Seismol Soc Am* 84(4):974–1002
- Whipp DM Jr, Ehlers TA, Blythe AE, Huntington KW, Hodges KV, Burbank DW (2007) Plio-Quaternary exhumation history of the central Nepalese Himalaya: 2. Thermokinematic and thermochronometer age prediction model. *Tectonics*. <https://doi.org/10.1029/2006TC001991>
- Wolff R, Hölzer K, Hetzel R, Xu Q, Dunkl I, Anczkiewicz AA, Li Z (2022) Spatially focused erosion in the High Himalaya and the geometry of the Main Himalayan Thrust in Central Nepal (85° E) from thermo-kinematic modeling of thermochronological data in the Gyirong region (southern China). *Tectonophysics* 834:229378
- Yamada M, Kandel T, Tamaribuchi K, Ghosh A (2020) 3D fault structure inferred from a refined aftershock catalog for the 2015 Gorkha Earthquake in Nepal. *B Seismol Soc Am* 110(1):26–37. <https://doi.org/10.1785/0120190075>
- Zhao B, Bürgmann R, Wang D, Tan K, Du R, Zhang R (2017) Dominant controls of down-dip afterslip and viscous relaxation on the postseismic displacements following the M W 7.9 Gorkha, Nepal, earthquake. *J Geophys Res-Solid* 122(10):8376–8401. <https://doi.org/10.1002/2017jb014366>

## Publisher's Note

Springer Nature remains neutral with regard to jurisdictional claims in published maps and institutional affiliations.

Submit your manuscript to a SpringerOpen® journal and benefit from:

- Convenient online submission
- Rigorous peer review
- Open access: articles freely available online
- High visibility within the field
- Retaining the copyright to your article

Submit your next manuscript at ► [springeropen.com](https://www.springeropen.com)